A Brief Overview of Models of Nucleon-Induced Reactions

B.V. Carlson

Depto. de Física, Instituto Tecnológico da Aeronáutica,

São José dos Campos, SP, Brazil

Abstract

The basic features of low to intermediate energy nucleon-induced reactions are discussed within the contexts of the optical model, the statistical model, preequilibrium and intranuclear cascade models. The calculation of cross sections and other scattering quantities are described.

These notes are a slightly revised version of lecture notes from the *Workshop on Nuclear Data for Science & Technology: Accelerator Driven Waste Incineration; Trieste, 10-21 September 2001,* provided here as supplementary material.

1 Introduction

A nuclear reaction is initiated when a nucleon or nucleus collides with another nucleon or nucleus. Reactions are characterized in first place by the incoming nuclei and the outgoing reaction products. Examples of the usual notation for this are ^{14}C(n,n)^{14}C, for the elastic scattering of neutrons on ^{12}C, ^{56}Fe(p,t)^{54}Fe, for the pickup by a proton of two neutrons from ^{56}Fe, and ^{235}U(n,n$'$) for inelastic neutron scattering from ^{235}U.

A complete description of a nuclear reaction involves other observable quantities beside the incoming nuclei and the outgoing reaction products. Among these are the relative energy of the incoming and outgoing nuclei and the scattering angle of the outgoing products. When the nuclei/nucleons involved have spin and/or excited states, their polarizations and/or excitation energies can also be observed.

The characteristics of the reactions induced by a given pair of incident nucleons/nuclei can be summarized in distributions of the occurrence of the reaction products, called cross sections. Quantitatively, the cross section σ_p for the production of a product p is defined as

$$\sigma_p = \frac{\text{number of particles p produced per unit time}}{\text{number of incident particles per unit time per unit area}} \,. \tag{1}$$

Cross sections have the dimension of area. The information obtained from cross sections often depends quite strongly on the internal structure of the initial and final nuclei. In fact, the comparison of experimental scattering observables with those obtained from various nuclear models can teach us a great deal about the structure of individual nuclei. After having used such a comparison to determine the model parameters appropriate for a given system, one hopes to use the same parameters to predict cross sections in other energy ranges or in neighboring systems.

2 Resonances

At low energies and for all but the lightest nuclear systems, nuclear reactions occur on two very distinct time scales. Direct reactions occur promptly, on a time scale of the same magnitude as the time it takes the projectile nucleus to pass by the target nucleus. Compound nuclear reactions, which involve the formation of a quasi-bound intermediate complex, occur on a time scale that is at least several orders of magnitude larger. A naive application of the uncertainty relation, $\Delta E \Delta t \geq \hbar$, would lead one to expect their energy scales to be inversely related. This is indeed the case. The contributions of direct reactions to the cross sections vary smoothly with energy. Compound nuclear reactions make contributions to the cross sections that fluctuate rapidly with energy.

The difference in the energy dependence of the direct and compound nucleus contributions to the cross section is clearly seen in Fig. 1, which displays the total neutron cross section on ^{58}Ni at extremely low incident neutron energy. One observes a direct reaction cross section – the result of elastic scattering of the neutron, in this case – that varies slowly with energy, except where it is punctuated by a faster variation due to the presence of a compound nuclear state of ^{59}Ni of about the same energy. At such low energies, separation of the direct and compound nucleus cross sections is a fairly straightforward (although often grueling) task.

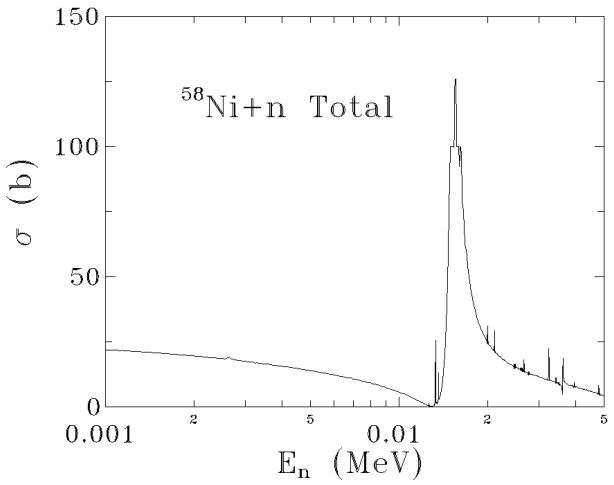

Figure 1: The total cross section for neutrons incident on ^{58}Ni at low incident energy, taken from the data of Ref. 1

2.1 Formalities

To formally separate the direct and compound nucleus contributions to the scattering, one begins by partitioning the Hilbert space of states into a component $\mathcal{P}$ containing the prompt states and an orthogonal component $\mathcal{Q}$ that contains the closed channels of the intermediate compound complex.[2] As a concrete example, one may consider $\mathcal{P}$ to be the subspace consisting of a nucleon scattering on ^{58}Ni, while $\mathcal{Q}$ consists of the ground and excited states of the nucleus ^{59}Ni (and other processes, such as γ emission or, in heavier nuclei, fission). The projection operators, P and Q, onto the subspaces $\mathcal{P}$ and $\mathcal{Q}$, respectively, which have the properties

$$\begin{aligned} P = P^\dagger \qquad & Q = Q^\dagger \\ P^2 = P \qquad & Q^2 = Q \\ P + Q = 1\,, & \end{aligned} \tag{2}$$

are then used to decompose the state vector of the system, Ψ, and its Schrödinger equation,

$$(E - H)\Psi = 0\,. \tag{3}$$

The prompt component of the state vector is $P\Psi$, while the slower component is $Q\Psi$, with

$$\Psi = P\Psi + Q\Psi\,. \tag{4}$$

We can multiply the Schrödinger equation on the left by P or by Q and use the decomposition of the wave vector to write the equation as two coupled equations,

$$(E - H_{PP})P\Psi = V_{PQ}Q\Psi \tag{5}$$

and

$$(E - H_{QQ})Q\Psi = V_{QP}P\Psi\,, \tag{6}$$

where

$$H_{PP} \equiv H_{0P} + V_{PP} \equiv PH_0P + PVP, \qquad V_{PQ} \equiv PHQ, \qquad \text{etc.},$$

and we have assumed that the contributions to the Hamiltonian of the internal degrees of freedom and the kinetic energy, both contained in H_0, do not couple the $\mathcal{P}$ and $\mathcal{Q}$ subspaces. We may formally solve the first of these, Eq.(5), as

$$P\Psi_c = \phi_c^{(+)} + \frac{1}{E^{(+)} - H_{PP}} V_{PQ} Q\Psi_c \,, \tag{7}$$

in which the (+) denotes an incoming wave boundary condition, the vector $\phi_c^{(+)}$ satisfies the Schrödinger equation in the $\mathcal{P}$ subspace,

$$(E - H_{PP})\phi_c^{(+)} = 0 \,, \tag{8}$$

with an incoming wave in channel c alone (and none in the $\mathcal{Q}$ subspace) and $P\Psi_c$ and $Q\Psi_c$ are the components of the full wave vector that evolve from this incoming wave. The solution $P\Psi_c$, when substituted into the second coupled equation, Eq. (6), yields

$$(E - H_{QQ} - W_{QQ})Q\Psi_c = V_{QP}\phi_c^{(+)} \,, \tag{9}$$

where

$$W_{QQ} \equiv V_{QP} \frac{1}{E^{(+)} - H_{PP}} V_{PQ} \,. \tag{10}$$

We can decompose the $\mathcal{P}$-subspace Greens function into its real and imaginary parts as

$$\frac{1}{E^{(+)} - H_{PP}} = \frac{P.P.}{E - H_{PP}} - i\pi\delta(E - H_{PP}) \,, \tag{11}$$

where $P.P.$ represents the principal part. The open channels in the $\mathcal{P}$ subspace thus make a negative imaginary contribution to W_{QQ}, which results in singularities in the wave vector in the lower half of the complex E plane.

Eq. (9) can be solved to obtain the $\mathcal{Q}$-subspace component of the wave vector as

$$Q\Psi_c = \frac{1}{E - H_{QQ} - W_{QQ}} V_{QP}\phi_c^{(+)} \,,$$

which then permits the expression of the $\mathcal{P}$-subspace component of the wave vector as

$$P\Psi_c = \phi_c^{(+)} + \frac{1}{E^{(+)} - H_{PP}} V_{PQ} \frac{1}{E - H_{QQ} - W_{QQ}} V_{QP}\phi_c^{(+)} \,. \tag{12}$$

2.2 Practical matters

At low relative energies, a collision between charged nuclei or a nucleus and a charged nucleon is dominated by the Coulomb force, which keeps the two beyond the range of nuclear interaction. Only neutrons can enter sufficiently close to a nucleus at such energies to feel the effects of the nuclear force.

Several factors also simplify the description of low-energy neutron scattering. The centripetal barrier keeps all but the l=0 s-wave contribution effectively out of the reach of the nuclear interaction for energies greater than about 50 keV. In addition, with few exceptions, nuclei have no excited states at energies lower than about 20 keV. The prompt component of neutron scattering then reduces to s-wave elastic scattering in this energy range.

The l=0 wave function satisfying an incoming wave boundary condition takes the form

$$\psi_0(r) = \frac{i}{2}(e^{-ikr} - S_0 e^{ikr}) \qquad\qquad r \to \infty\,. \tag{13}$$

where the wavenumber is $k = \sqrt{2\mu E_{cm}/\hbar^2}$, μ is the reduced mass and E_{cm} the center-of-mass energy.

The wave vector of Eq. (12) yields an l=0 S-matrix S_0 that can be approximated in a multi-level Breit-Wigner form (among others) as

$$S_{0,ab} = e^{i(\phi_a+\phi_b)}\left(\delta_{ab} - i\sum_\mu \frac{g_{\mu a}\, g_{\mu b}}{E - \varepsilon_\mu + i\Gamma_\mu/2}\right)\,, \tag{14}$$

where ϕ_a and ϕ_b are the initial and final channel phase shifts and the amplitude $g_{\mu c}$ characterizes the coupling of the compound state μ to the channel c, with $\Gamma_\mu = \sum_j g_{\mu c}^2$.

The first term in this expression is the direct scattering amplitude associated with scattering in the $\mathcal{P}$ subspace alone. The second term describes the slower processes that result from coupling through the states of the $\mathcal{Q}$ subspace. The first term varies slowly as a function of energy while the second term varies rapidly. The resonance energies ε_μ are not identical to the energies of the compound nuclear states due to the energy shift given by the real part of Eq. (11). The amplitudes $g_{\mu c}$ can be positive and negative and, after extracting an appropriate penetration factor, are distributed normally (with few exceptions).

Once the S-matrix is known, the cross sections can be calculated. For the case of s-wave scattering on a spin zero target, the cross sections directly related to the elastic channel S-matrix element, $S_{0,aa}$, are the total, elastic and absorption ones,

$$\begin{aligned} \sigma_{tot} &= \frac{2\pi}{k^2}(1 - \mathrm{Re}\, S_{0,aa})\,, \\ \sigma_{el} &= \frac{\pi}{k^2}\left|S_{0,aa} - 1\right|^2\,, \\ \text{and} \qquad \sigma_{abs} &= \frac{\pi}{k^2}(1 - |S_{0,aa}|^2) = \frac{\pi}{k^2}T_0\,, \end{aligned} \tag{15}$$

where T_0 is the s-wave transmission coefficient. The reaction cross section and the transmission coefficient T_0 are non-zero when the elastic S-matrix element $S_{0,aa}$ is smaller than one in

magnitude. This occurs when flux is passed through the long-lived compound-nucleus states to other channels, such as γ emission or fission. The cross section for these take the form

$$\sigma_{ac} = \frac{\pi}{k^2} \left| S_{0,ca} \right|^2 .$$

One can easily verify that the total flux is conserved,

$$\sigma_{abs} = \sum_{j \neq i} \sigma_j \qquad \text{and} \qquad \sigma_t = \sigma_{el} + \sigma_{abs} .$$

At extremely low energies, below the resonance region, the elastic cross section is observed to approach a constant value, σ_{el}^0. This value is used to calculate another quantity of physical interest, the scattering radius, $R' = \sqrt{\sigma_{el}^0 / 4\pi}$.

Although only s-wave resonances have been discussed here, p-wave resonances are also observed quite frequently (the narrow peaks in Fig. 1, for example) and even d-wave resonances are observed in some cases. Due to the centripetal barrier, their partial widths are much smaller than those of s-wave resonances. However, when the appropriate penetration factor is extracted from the amplitudes $g_{\mu j}$ of these resonances, they too are distributed normally. The interested reader can find a much more detailed description of nuclear resonance reactions in Refs. [3] and [4].

3 The optical model

At higher energies, the density of compound nucleus states becomes so large that the individual contributions can no longer be resolved. It then becomes impossible to distinguish the slow energy dependence of the direct contribution from the rapid variations of the compound nucleus one. An example of this is given in Fig. 2, where the total cross section for neutrons incident on ^{58}Ni is again shown, but now at higher energies. The fluctuations in the cross section, called Ericson fluctuations,[6] do not permit the determination of the contribution to the cross section of each individual compound nuclear state. Instead, only the average properties of the compound nucleus contribution to the cross section can be determined. It is in this context that the optical potential plays a crucial role in the separation of the two contributions.

The principal objective of the optical model is to describe just the prompt, direct reactions in a nuclear collision. To separate the direct reactions from the compound-nucleus ones (theoretically), one assumes that the compound-nucleus reactions do not contribute to the average wave function and scattering amplitudes, due to their rapid fluctuations in energy. Note that the compound-nucleus reactions still DO contribute to the average cross sections, which are, for the most part, proportional to the squares of the amplitudes. The energy-averaged amplitudes, however, are associated with the scattering amplitudes for the prompt component of the scattering. The optical model potential is defined as the potential which furnishes the energy-averaged scattering amplitudes.

In a wider context, the optical potential can be considered an effective potential that takes into account all of the physical processes one does not want to take into account explicitly. The most important of these are the rapidly fluctuating compound-nucleus contributions

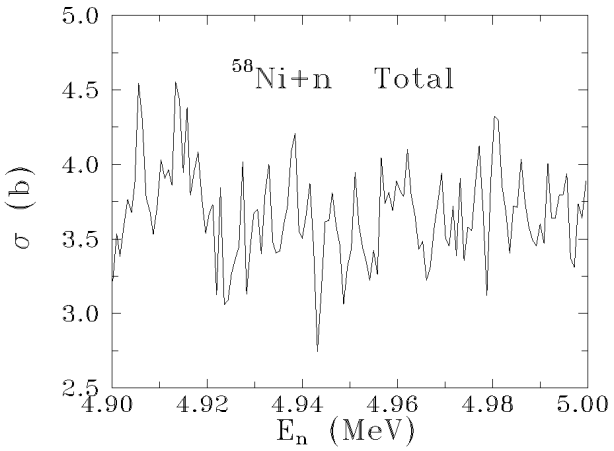

Figure 2: The total cross section for neutrons incident on ^{58}Ni in a small incident energy range close to 5 MeV, taken from the data of Ref. 2

to the scattering. But direct processes are also included at times. One example of this is the use of an effective spherical optical model potential to take into account the coupling to excited states of the target. Another example is the deuteron optical potential, which usually contains the contribution of direct deuteron breakup.

As well as being fundamental for the calculation of direct reaction observables, optical model calculations are also used to produce the transmission coefficients essential for the analysis of compound nucleus cross sections within the Hauser-Feshbach statistical theory. They are thus one of the first and most important steps in the evaluation of nuclear cross sections.

3.1 Formalities

Returning to the $\mathcal{P}$-subspace wave vector of Eq. (12), one can write its energy average as

$$\langle P\Psi_i \rangle = \phi_i^{(+)} + \frac{1}{E^{(+)} - H_{PP}} V_{PQ} \left\langle \frac{1}{e_{QQ}} \right\rangle V_{QP} \phi_i^{(+)} \,, \tag{16}$$

since

$$e_{QQ} = E - H_{QQ} - W_{QQ} \tag{17}$$

is the only rapidly varying function of the energy in the expression. The average wave vector can be written in a Schrödinger-equation-like form by multiplying both sides of the expression, Eq. (16), by $E^{(+)} - H_{PP}$,

$$(E - H_{PP}) \langle P\Psi_i \rangle = V_{PQ} \left\langle \frac{1}{e_{QQ}} \right\rangle V_{QP} \phi_i^{(+)} \,. \tag{18}$$

Using Eq. (16) again to rewrite the wave vector $\phi_i^{(+)}$ as

$$\phi_i^{(+)} = \frac{1}{1 + (E^{(+)} - H_{PP})^{-1} V_{PQ} \langle 1/e_{QQ} \rangle V_{QP}} \langle P\Psi_i \rangle \,, \tag{19}$$

substituting this in Eq. (18) and performing a bit of algebra, one finally obtains the optical model equation,

$$\left[E - H_{PP} - V_{PQ}\frac{1}{\langle 1/e_{QQ}\rangle^{-1} + W_{QQ}}V_{QP}\right]\langle P\Psi_i\rangle = 0\,. \tag{20}$$

The optical potential can thus be written as

$$V_{opt} = V_{PP} + V_{PQ}\frac{1}{\langle 1/e_{QQ}\rangle^{-1} + W_{QQ}}V_{QP}\,. \tag{21}$$

To conclude the formal development of the optical model, one must evaluate the average value $\langle 1/e_{QQ}\rangle$. The simplest way of doing this is to average the quantity $1/e_{QQ}$ over a normalized Lorentzian density,

$$\left\langle \frac{1}{e_{QQ}} \right\rangle = \int dE_0\, \frac{\rho(E, E_0)}{E_0 - H_{QQ} - W_{QQ}}\,, \tag{22}$$

where

$$\rho(E, E_0) = \frac{\Delta}{2\pi}\frac{1}{(E - E_0)^2 + (\Delta/2)^2}\,. \tag{23}$$

Assuming the quantity $1/e_{QQ}$ to have no poles in the upper half of the complex E plane (due to causality, it should have them only in the lower half-plane), one can perform the integral by closing the contour and calculating residues in the upper half plane to obtain

$$\left\langle \frac{1}{e_{QQ}} \right\rangle = \frac{1}{E + i\Delta/2 - H_{QQ} - W_{QQ}}\,, \tag{24}$$

and hence

$$U_{opt} = V_{PP} + V_{PQ}\frac{1}{E - H_{QQ} + i\Delta/2}V_{QP}\,. \tag{25}$$

The optical potential is obviously energy-dependent, non-local and complex due to the energy-averaged propagator $(E - H_{QQ} + i\Delta/2)^{-1}$ in the second term. Its imaginary part is negative, resulting in a potential that is absorptive. The flux of particles leaving the scattering region is smaller than the incident flux, with the remaining fraction of the flux being absorbed by the potential. It is through its imaginary part that the optical potential takes into account the flux that is lost from the states of the $\mathcal{P}$ subspace to the states of the $\mathcal{Q}$ subspace.

3.2 Neutron optical scattering at low energy

As argued above, the prompt component of neutron scattering at low energies reduces to s-wave elastic scattering in this energy range. The optical model equation for the s-state wave function ψ_0 is

$$(E_{cm} - T - U_{opt})\frac{\psi_0}{r} = 0\,. \tag{26}$$

To solve this equation numerically, one develops the solution, $\psi_{0,int}(r)$, starting from $r = 0$, using the condition that the wave function vanishes at the origin, $\psi_{0,int}(r = 0) = 0$ and one of many possible numerical methods (Cowell, Numerov, modified Numerov, Runge-Kutta, etc.). The equation is solved numerically out to a radius r_m, beyond which the optical potential can be neglected. For values of the radius equal to or larger than this matching radius, the solution to the differential equation that satisfies the incoming wave boundary condition takes the form

$$\psi_{0,ext}(r) = \frac{i}{2}(e^{-ikr} - \bar{S}_0 e^{ikr}) \qquad\qquad r \geq r_m \,. \tag{27}$$

One requires, at the matching radius r_m, that this external wave function and its derivative be the continuous extensions of the numerical wave function obtained in the the internal region and of its derivative. This results in two equations, whose solution yields the amplitude of the internal wave function and the S-matrix element, $\bar{S}_0$.

Once the S-matrix is known, the optical cross sections can be calculated. For the case of s-wave scattering on a spin zero target, these are again the total, elastic and absorption cross sections,

$$\begin{aligned} \sigma_{tot} &= \frac{2\pi}{k^2}(1 - \mathrm{Re}\,\bar{S}_0)\,, \\ \sigma_{el} &= \frac{\pi}{k^2}\left|\bar{S}_0 - 1\right|^2\,, \\ \text{and} \qquad \sigma_{abs} &= \frac{\pi}{k^2}(1 - \left|\bar{S}_0\right|^2) = \frac{\pi}{k^2}T_0\,, \end{aligned} \tag{28}$$

where T_0 is the s-wave transmission coefficient. The absorption cross section and the transmission coefficient T_0 are non-zero when the S-matrix element $\bar{S}_0$ is smaller than one in magnitude. This occurs when flux is absorbed by the long-lived compound-nucleus states. Care must be taken, however, when comparing the optical model absorption cross section to the experimental reaction cross section. A part of the flux absorbed by the compound nucleus can later be re-emitted in the elastic channel, in which case it should rightly be considered part of the elastic cross section.

Of the three optical cross sections, only the total one can be compared directly with experimental data, as it is the only one that is linear in the scattering amplitude (here the S-matrix element $\bar{S}_0$). The S-matrix element can be written in general as the sum of an average and a fluctuating part, $S = \bar{S} + S_{fl}$. The average elastic cross section then has the form

$$\langle\sigma_{el}\rangle = \frac{\pi}{k^2}\left|\bar{S} - 1\right|^2 + \frac{\pi}{k^2}\left\langle\overline{|S_{fl}|^2}\right\rangle\,. \tag{29}$$

The first term alone gives the elastic cross section of the optical model. The average value of the fluctuating term is calculated within the statistical model.

In the resonance region, s-wave and p-wave strength functions can be defined. The s-wave strength function, s_0, relates the average neutron partial width $\langle\Gamma_0\rangle$ and spacing D_0 of the resonances to the optical model absorption. One has, approximately,

$$s_0 = \frac{\langle\Gamma_0\rangle}{D_0}\left(\frac{E_0}{E_{cm}}\right)^{1/2} \approx \frac{1 - |\bar{S}_0|^2}{2\pi\sqrt{E_{cm}}}\,, \tag{30}$$

where E_0 is usually taken to be 1 eV. The factor $\sqrt{E_{cm}}$, the s-wave penetrability, cancels the energy dependence of the neutron partial width, so that the strength function varies slowly with the incident neutron energy. The p-wave strength function, s_1, relating the average partial width and spacing of the $l = 1$ resonances is defined analogously in terms of the p-wave S-matrix elements and penetrability.

Adjustment of the optical model parameters at low energy to reproduce the s-wave and p-wave strength functions, the scattering radius and the total cross section is known as the SPRT method.[7] A good fit to these observables is important in determining the low energy behavior of the optical cross sections and the transmission coefficients, which is important, in turn, in determining the behavior of compound nucleus cross section calculations near threshold.

3.3 The phenomenological optical potential

The formal derivation of the optical potential might suggest that it could be calculated directly. Although a good deal of work has indeed been done in this direction, the resulting potentials are often difficult to calculate and still not sufficiently precise. They also have the drawback of being non-local, which can greatly complicate solution of the corresponding Schrödinger equation.[8, 9, 10, 11]

Instead, phenomenological optical model potentials are normally used to compare and fit to experimental data. With few exceptions, these potentials are taken to be local. However, the qualitative characteristics of the geometry and the general trend of the energy dependence of the phenomenological potentials are quite similar to those found in microscopic potentials. Both types of potentials are, after all, trying to describe the same physical processes.

In the empirical potentials, the functional form is usually determined by a limited set of parameters that are adjusted to obtain a best fit with the experimental data. Over the years, a standard form of the phenomenological optical model potential has evolved, which permits the parametrization of the scattering of a light particle (neutron, proton, deuteron, triton, ^{3}He or alpha) from a given nucleus. This is

$$\begin{aligned} U_{opt}(r) = \quad & +V_C(r) && \text{a Coulomb term,} \\ & -(V + iW)\, f_{V,W}(r) && \text{a complex volume term,} \\ & +(V_s - iW_s) g_{V_s,W_s}(r) && \text{a complex surface term,} \\ & -d_{so}\, \vec{l} \cdot \vec{s}\, (V_{so} + iW_{so})\, h_{V_{so},W_{so}}(r) && \text{a complex spin} - \text{orbit term,} \end{aligned} \tag{31}$$

where the spin-orbit constant is $d_{so} = (\hbar/m_\pi c)^2 \approx 2$ fm^2, m_π being the pion mass.

The Coulomb term is usually taken to be the interaction of a projectile point charge Z_p with a uniformly charged target sphere of radius R_c and total charge Z_t. Although this potential neglects the surface diffusivity of the nuclear charge distribution, it is a reasonable approximation in the case of the scattering of light particles from nuclei.

The real and imaginary volume terms are normally taken to be of Wood-Saxon form,

$$f_i(r) = \frac{1}{1 + \exp\left[(r - R_i)/a_i\right]} \qquad i = V, W, \tag{32}$$

where R_i and a_i are the radii and the diffusivities, respectively, of the two terms. The Wood-Saxon form factor can be thought of as a smoothed step function, falling from one for values of the radius r smaller than the radius R_i to zero for values of r greater than R_i, in a few multiples of the diffusivity a_i.

The real volume potential reflects the average interaction of the projectile with the nucleons of the target nucleus. The Wood-Saxon form factor it uses is quite similar in form to the nucleon density of a saturated nucleus ($A \geq 30$). (For lighter nuclei, a Gaussian geometry is sometimes used.) The strength of the real volume potential is roughly proportional to the mass of the projectile and decreases with the incident energy, in qualitative agreement with the results of calculations of the nuclear mean field.[12]

The imaginary volume potential takes into account the loss of projectile particles due to collisions with the nucleons of the target. It is zero at low energies, for which the projectile does not have sufficient energy to excite single nucleon modes. At higher energies, it increases slowly with the incident energy, as the phase space available for single nucleon excitation increases. At even higher energies, both the real and imaginary volume potentials for nucleon scattering are fairly well described by the impulse approximation, in which the the target density is simply folded with the nucleon-nucleon cross section.[13, 14]

The real and imaginary surface terms of the optical potential are taken to be either the derivative of a Wood-Saxon,

$$g_i(r) = -4a_i \frac{d}{dr} f_i(r) \qquad\qquad i = V, W, \tag{33}$$

or a Gaussian. In either case, the potential peaks at a radius R_i and falls to zero within a few multiples of the diffusivity a_i. A derivative Wood-Saxon form factor with diffusivity a_{WS} is almost indistinguishable from a Gaussian form factor with diffusivity $a_G = 2.21 a_{WS}$.

The imaginary surface term of the optical potential takes into account the absorption due to the coupling to the quasi-bound compound nucleus states and to the excitation of low-energy collective modes, which have their couplings concentrated in the nuclear surface. Similar many-body effects can also be invoked to justify the presence of a real surface term. However, given the imaginary surface term, the existence of the real term can be shown to follow directly, by using a dispersion relation based on the causality of the optical potential (no singularities in the energy upper halfplane).[15] The dispersion relation shows that an energy-dependent imaginary potential $W(r, E)$ necessarily leads to a contribution $\Delta V(r, E)$ to the real potential. If the imaginary term is a surface one, the real term resulting from the dispersion relation will be a surface one as well.

Both the real and imaginary spin-orbit terms of the optical potential are taken to have a Thomas form factor,

$$h_i(r) = -\frac{1}{r} \frac{d}{dr} f_i(r) \qquad\qquad i = V_{so}, W_{so}. \tag{34}$$

Like the surface imaginary term, the Thomas form factor yields potentials which peak at a radius near R_i and fall to zero in a few multiples of the diffusivity a_i.

The Thomas form factor, as well as the spin-orbit potential itself, can be derived (for spin 1/2 particles) by performing a reduction of a Dirac equation with Wood-Saxon potentials

to an equivalent Schrödinger equation.[12] The spin-orbit interaction and the Thomas form factor can then be interpreted as but another manifestation of the volume interaction of the incident particle with the nucleons of the target nucleus.

The phenomenological optical potential is thus parametrized in terms of a set of potential strengths and corresponding geometrical parameters. These parameters have been adjusted to experimental data for many systems and many values of the relative energy. Several attempts have been made to adjust a single set of parameters to a wide range of systems by introducing a dependence on the target charge and mass as well as that on the relative energy. The potentials obtained using such sets of parameters are called global optical potentials. Many individual and global optical parameter sets can be found in an old compilation by Perey and Perey.[16] However, the best modern reference for optical potential parameters is the Reference Input Parameter Library (RIPL), available both online and in CD from the Internationational Atomic Energy Agency.[17]

For nucleons, typical values of the potential strengths are

$$\begin{array}{lll} V \approx & (45-55)\ \text{MeV} - (0.2-0.3)E\,, & \\ W_s \approx & (2-7)\ \text{MeV} + (0.3-0.5)E & E < 8-10\ \text{MeV}, \\ V_{so} \approx & (4-10)\ \text{MeV}. & \end{array} \tag{35}$$

Above 8 – 10 MeV, W_s is usually constant or slightly decreasing. V_s and W_{so} can normally be taken to be zero as can W below about 10 MeV. Above about 10 MeV, W is constant or slightly increasing. At sufficiently high energies, typically about 300 MeV, the optical potential strength V changes sign, becoming repulsive. As mentioned above, for heavier particles, the real volume potential V scales approximately linearly with the mass.

The radii R_i characteristically take on values close to that of the radius of the target matter distribution. They are often parameterized in terms of reduced radii r_i and the target mass as $R_i = r_i A_t^{1/3}$, with the reduced radii in the range $r_i \approx 1.2$ - 1.3 fm. The diffusivities normally take on values in the range $a_i \approx 0.4$ - 0.7 fm, except in the case of a Gaussian surface form factor, for which the typical values are slightly larger.

Not all of the optical model parameters are uniquely determined by the experimental data. It has been observed, for example, that fairly wide ranges of the parameters V, R_v, W_s, and a_s result in equally good fits to the experimental data if the values of VR_v^2 and $W_s a_s$ remain constant. These are known as potential ambiguities.

3.4 Partial wave expansion in the single-channel optical model

When angular momenta greater than the s-wave contribute to the scattering, the wave function and the scattering matrix are determined most conveniently when decomposed in angular momentum partial waves. The partial wave expansion of the scattering wave function of a particle of spin s [18] can be written as

$$\Psi = \frac{4\pi}{kr} \sum_{ljn} i^l\, e^{i\sigma_l} \psi_l^j(r) \mathcal{Y}_{ls}^{jn}(\hat{r}) \mathcal{Y}_{ls}^{jn\dagger}(\hat{k})\,, \tag{36}$$

in terms of the spin-angular functions

$$\mathcal{Y}_{ls}^{jn}(\hat{r}) = i^l \sum_{m\nu} \langle s\nu lm|jn\rangle\, Y_{lm}(\hat{r})\, |s\nu\rangle\ , \tag{37}$$

where l and j are the orbital and total angular momenta and $|s\nu\rangle$ is an eigenvector of the particle spin. In the expansion of the wave function, σ_l is the Coulomb phase, $\hat{r}$ denotes the angular variables and $\hat{k}$ the direction of the incident momentum. (The S-matrix element in partial wave l for pure Coulomb scattering of the projectile from the target would be $e^{2i\sigma_l}$.) The factor $i^l e^{i\sigma_l}\psi_l^j(r)/kr$ could have been written as simply $\psi_l^j(r)$ in the partial wave expansion. The form used above simplifies subsequent manipulations.

When the partial-wave expansion of the wave function is substituted in the optical Schrödinger equation, one can extract an independent equation for the wave function ψ_l^j in each partial wave. The incoming-wave boundary condition requires that asymptotically the wave function take the form of an incoming plane wave and an outgoing scattering wave. To be consistent with this and satisfy the differential equation, the wave function ψ_l^j must have the asymptotic form,

$$\psi_l^j(r) \to \frac{i}{2}\left(H_l^-(r) - H_l^+(r)e^{2i\sigma_l}\,S_l^j\right)e^{-i\sigma_l}\,, \tag{38}$$

where $H_l^\pm$ are the linear combinations of the regular and irregular Coulomb wave functions that asymptotically contain only incoming (H_l^-) or outgoing (H_l^+) waves. S_l^j is the nuclear part of the S-matrix element and $e^{2i\sigma_l}$ the Coulomb part.

The S-matrix elements, S_l^j, are obtained in the same manner as $\bar{S}_0$ is obtained in the case of low-energy neutron scattering. In the internal region, the differential equation for each partial wave is solved numerically out to the radius, r_m. The numerical solution and its derivative are matched there to the wave function in the external region, given by Eq. (38), and to its derivative, to obtain the ampitude in the internal region, a_l^j, and the S-matrix element, S_l^j.

The only novelty to the solution here is deciding with which partial wave to stop the calculation, for l and j extend to infinity. The calculation is normally stopped when the nuclear S-matrix elements are sufficiently close to one. This occurs when the centripetal barrier no longer permits the projectile to enter the range of nuclear interaction with the target. For partial waves of larger l, the scattering reduces to pure Coulomb scattering (or for neutrons, no scattering at all), as is evident from Eq. (38).

When the asymptotic form of the partial wave function, ψ_l^j, of Eq. (38), is substituted in the partial wave expansion of the total wave function, Eq. (36), one can extract the partial wave expansion of the scattering amplitude,

$$f(\theta) = \frac{4\pi}{2ik}\sum_{ljn}\left(e^{2i\sigma_l}\,S_l^j - 1\right)\mathcal{Y}_{ls}^{jn}(\hat{r})\mathcal{Y}_{ls}^{jn\dagger}(\hat{k})\,. \tag{39}$$

For spin-1/2 particles, the scattering amplitude is a 2x2 matrix (corresponding to the two projections of the spin) with two distinct amplitudes.

The differential elastic cross section for an unpolarized incident beam is obtained by averaging the squared magnitude of the scattering amplitudes over the initial values of the projectile spin and summing over the final ones. The general expression that results is

$$\frac{d\sigma}{d\Omega} = \frac{1}{2s+1}\sum_{\nu\nu'}\left|f_{\nu'\nu}(\theta)\right|^2\,. \tag{40}$$

For particles of spin-1/2 and greater, one can define vector and tensor spin observables in terms of other combinations of the amplitudes.

The fraction of flux absorbed from each partial wave is given by the transmission coefficient, T_l^j, defined as

$$T_l^j = 1 - \left|S_l^j\right|^2 . \tag{41}$$

When the S-matrix element is unitary, no flux is absorbed and the transmission coefficient is zero. When absorption is complete, the transmission coefficient is one. These quantities are essential for calculating statistical cross sections. Quite often, optical model calculations are a mere preliminary to statistical model calculations and are performed only to obtain the transmission coefficients.

The total flux lost in the scattering is related to the absorption cross section through the equation

$$\sigma_{abs} = -\frac{1}{v} \oint \vec{j} \cdot d\vec{a} \,, \tag{42}$$

where it is understood that the probability current,

$$\vec{j} = \frac{\hbar}{2i\mu} \left(\Psi^\dagger \nabla \Psi - (\nabla \Psi^\dagger) \Psi \right) , \tag{43}$$

is integrated over a surface which tends to infinity. The absorption cross section can be expressed in terms of the transmission coefficients as

$$\sigma_{abs} = \frac{1}{2s+1} \frac{\pi}{k^2} \sum_{lj} (2j+1)\, T_l^j \,. \tag{44}$$

For charged particles, integration of the differential elastic cross section of Eq. (40) leads to an infinite result, due to the infinite range of the Coulomb interaction. For neutrons, it yields the elastic cross section,

$$\sigma_{el} = \int d\Omega \, \frac{d\sigma}{d\Omega} = \frac{\pi}{2k^2} \sum_{lj} (2j+1) \left|1 - S_l^j\right|^2 . \tag{45}$$

This is often called the shape elastic cross section to distinguish it from the compound elastic one, which describes re-emission into the elastic channel from the compound nucleus.

For neutrons, a total cross section can also be defined as the sum of the elastic and absorption cross sections,

$$\sigma_{tot} = \sigma_{el} + \sigma_{abs} = \frac{\pi}{k^2} \sum_{lj} (2j+1)(1 - \mathrm{Re}\, S_l^j) \,. \tag{46}$$

The total cross section takes into account all flux lost from the incident plane wave. Comparing the expression for the total cross section with that of the scattering amplitude, $f(\theta)$, one sees that the optical theorem is explicitly verified by the partial wave expansion,

$$\sigma_{tot} = \frac{4\pi}{k} \mathrm{Im}\, f(\theta = 0^\circ) \,. \tag{47}$$

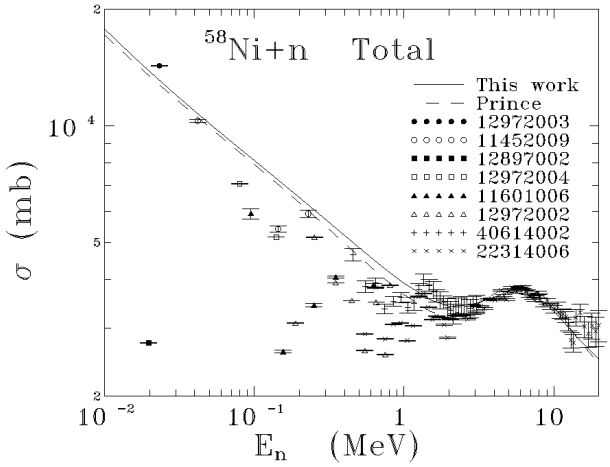

Figure 3: Various experimental measurements of the n+^{58}Ni total cross section, identified by their EXFOR access numbers, are shown together with two optical model calculations.

As noted earlier, when it exists, the total optical cross section is the average of an amplitude and can thus be compared directly with the energy-averaged experimental data. This is done in Fig. 3, where a selection of the experimental measurements of the $n + ^{58}\,Ni$ total cross section is shown together with optical model calculations using the parameters of A. Prince[19] and another set. Although there is a great deal of dispersion in the low energy data, the calculations follow its trend.

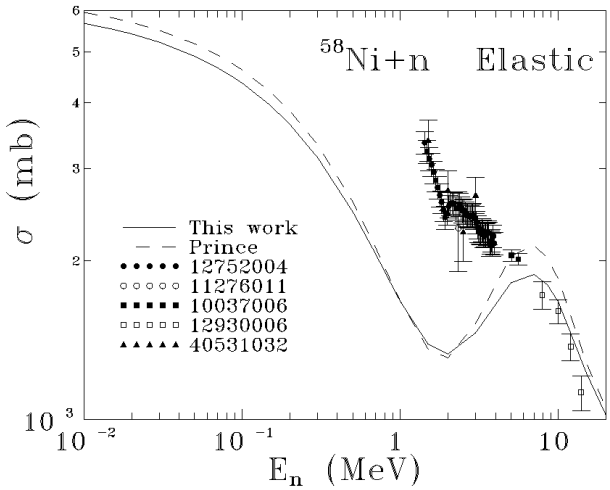

Figure 4: Various experimental measurements of the n+^{58}Ni elastic cross section, identified by their EXFOR access numbers, are shown together with two optical model calculations.

The optical elastic and absorption cross sections involve the average of a squared amplitude and cannot be compared directly with the energy-averaged experimental data. The compound elastic cross section is part of the optical reaction cross section rather than the elastic cross section. The experimental elastic cross section can thus greatly exceed the optical component of the cross section. This is illustrated in Fig. 4, in which a selection of the experimental measurements of $n + ^{58}\,Ni$ are compared to optical model calculations using

the same optical parameters as above. At energies high enough for the elastic compound nucleus cross section to have dropped to zero (usually at an energy of the order of a few MeV), the differential and integral (when it exists) optical elastic cross sections can be compared with the energy-averaged experimental data. Note that the elastic cross section for neutron-induced scattering can also be compared to the experimental data at extremely low incident energies, where it is customarily expressed as a scattering radius R'.

At high energies, the absorption cross section can also be compared to experimental reaction cross section data. However, the reaction cross section cannot be measured directly, making the data for such a comparison scarce.

3.5 The generalized optical potential

The single-channel or spherical optical model treates the target nucleus as if it were spherical. But nuclei are often deformed. Even those that are spherical are often susceptible to shape oscillations. Deformed and vibrational nuclei possess low-lying collective states that are easily excited in a collision. As these excitations are prompt reaction modes, one would expect their description to lie within the scope of a generalized optical model. The standard extension of the optical model takes into account the expected deviation from spherical symmetry by modifying the radii R_i of the terms in the optical model potential.

Evey nucleus possesses vibrational excitation modes in which the excited states undergo shape oscillations about the equilibrium form.[20] In a nucleus with a spherically symmetric ground state, the excited states of lowest energy are vibrational excitations. To include these modes in an optical model description, the radii of the different contributions to the potential are expressed in terms of the creation and annihilation operators of the nuclear phonons and the amplitudes of their respective shape oscillations. One usually expands the optical potential to first or second order in the creation and annihilation operators, thereby taking into account the direct excitation of one- and two-phonon states.

The nucleus ^{58}Ni serves as an example of a typical vibrational nucleus. Two neutrons from a doubly magic configuration, it has a spherically symmetric $J = 0^+$ ground state and a $J = 2^+$ excited state at E_x=1.454 MeV that can be considered a one-quadrupole-phonon vibrational state. At about twice the energy of the one-phonon state, in particular, at E_x=2.459, 2.776, and 2.943 MeV, one finds a trio of states with $J = 4^+$, 2^+, and 0^+, respectively, which can be interpreted as the two-phonon states. The fact that the first two these (but not the third) decay almost exclusively to the $J = 2^+$ excited state corroborates such an interpretation, but also shows its limitations.

A statically deformed nucleus possesses rotational excited states.[20] In this case the radii R_i of the optical potential are replaced by an angle-dependent form expressing the static deformation, yielding a potential that depends on the orientation of the target. When the deformation of the nucleus is large, expansion of the optical potential in a Taylor series is not a good approximation. It is better to expand it directly in multipoles of the relative angle between the projectile and the orientation of the target.

The nucleus ^{238}U provides an excellent example of a statically deformed nucleus with rotational excitations. Its 0^+ ground state possesses static quadrupolar e hexadecapolar deformations with $\beta_2 = 0.198$ and $\beta_4 = 0.057$. Its first four excited states, at $E_x - J^\pi =$

0.044 MeV-2^+, 0.148 MeV-4^+, 0.307 MeV-6^+, and 0.518 MeV-8^+, iniciate a rotational band that can be traced to at least the 28^+ state at E_x=4.516 MeV. Each of these states decays exclusively to the next lower state in the rotational band.

The introduction of target degrees of freedom leads to a generalized optical potential that depends on the relative orientation of the target with respect to the projectile. The system is no longer invariant under independent rotations of the target or the projectile and their individual angular momenta are not conserved. However, in all cases, the system continues invariant under a simultaneous rotation of the projectile and target. The total angular momentum thus continues to be a conserved quantity.

The partial wave expansion proceeds in the coupled-channels optical model much as it did in the single-channel one. There are several new features however. The first of these is that the excited states and their angular momentum must now be taken into account. The wave function in a partial wave of total angular momentum J and parity π is then not a scalar, as it is in the spherical model (for projectiles of spin 0 or 1/2), but a matrix. The differential equation that must be solved is also a matrix one. Although the only solution that is normally of interest is the one in which the target is in its ground state in the incoming wave, the complete matrix solution is needed to invert the matching equations and obtain the S-matrix, which is now a matrix, $S_{l'j'c',ljc}$, labeled by the orbital and total angular momenta of the projectile, l and j, and by the target state c. The calculation is thus much more time consuming than in the spherical case.

To obtain the partial wave expansion of the scattering amplitude, one repeats the procedure used earlier: substitute the asymptotic form of the partial wave function, Ψ_J in the partial wave expansion of the total wave function and compare the result to the expected form of the asymptotic wave function. Once the scattering amplitude is known, calculating cross sections is a simple matter. The differential cross sections for an unpolarized incident beam and target are obtained by averaging the squared magnitude of the scattering amplitudes over the initial values of the projectile and target spin and summing over the final values. The differential cross section for a collision, in which the target of spin I_a initially in its ground state a is scattered to a final (ground or excited) state c, is given by

$$\frac{d\sigma_{ac}}{d\Omega} = \frac{1}{(2s+1)(2I_a+1)} \sum_{\substack{\nu' M_c \\ \nu M_a}} \left| f_{\nu' c M_c, \nu a M_a}(\theta) \right|^2 , \tag{48}$$

where ν, ν' and M_a, M_c are the initial and final projections of the projectile and target spins, respectively. The elastic optical angular distribution is forward peaked when the scattering involves partial waves above the s-wave. The inelastic angular distributions need not be.

Due to the infinite range of the Coulomb force, the integrated elastic cross section is finite only when at least one of the two colliding particles is neutral. In the particular case of neutrons incident on a nucleus, integration of the differential cross section yields,

$$\sigma_{el} = \frac{1}{2(2I_a+1)} \frac{\pi}{k^2} \sum_{\substack{l'j'lj \\ J}} (2J+1) \left| S^J_{l'j'a,lja} - \delta_{l'l}\delta_{j'j} \right|^2 . \tag{49}$$

The integrated inelastic cross sections exist for for both neutral and charged particles. They

take the form

$$\sigma_{ac} = \frac{1}{(2s+1)(2I_a+1)} \frac{\pi}{k^2} \sum_{\substack{l'j'lj \\ J}} (2J+1) \left| S^J_{l'j'c,lja} \right|^2 \qquad c \neq a \,. \tag{50}$$

In the coupled-channel problem, it is also possible to define an absorption cross section, which can be related to the total flux lost from all channels, elastic and inelastic, as

$$\sigma_{abs} = -\frac{1}{v} \oint \sum_c \vec{j}_c \cdot d\vec{a} \,, \tag{51}$$

where the probability current in channel c,

$$\vec{j}_c = \frac{\hbar}{2i\mu} \left(\Psi_c^\dagger \nabla \Psi_c - (\nabla \Psi_c)^\dagger \Psi_c \right) \,, \tag{52}$$

is integrated over a surface which tends to infinity, with Ψ_c the component of the wave function that asymptotically occupies state c. Using the asymptotic form of the partial waves, the expression for the absorption cross section can be reduced to

$$\sigma_{abs} = \frac{1}{(2s+1)(2I_0+1)} \frac{\pi}{k^2} \sum_{ljJ} (2J+1)\, T^J_{lja,lja} \,, \tag{53}$$

where the coupled-channels transmission coefficients have been introduced. These are defined in terms of the S-matrix S^J as[21]

$$T^J = 1^J - S^{J\dagger} S^J \,. \tag{54}$$

The total flux lost from the elastic channel can also be related to a reaction cross section through the restriction of Eq. (51) to the ground state component,

$$\sigma_r = -\frac{1}{v} \oint \vec{j}_a \cdot d\vec{a} \,. \tag{55}$$

This expression can be reduced to a form similar to that of Eq. (53), but involving only the squared magnitudes of the ground state S-matrix elements. Comparison of the form of the reaction and absorption cross sections reveals a simple relation between the two,

$$\sigma_r = \sigma_{abs} + \sum_{c \neq a} \sigma_{ac} \,. \tag{56}$$

In other words, the elastic channel loses flux to both the prompt inelastic channels and the long-lived compound states. The reaction cross section takes both of these into account.

For neutral particles, the neutron in particular, the elastic cross section is finite. A total cross section can then be defined as the sum of the elastic and reaction cross sections,

$$\sigma_{tot} = \sigma_{el} + \sigma_r = \frac{1}{2I_a+1} \frac{\pi}{k^2} \sum_{ljJ} (2J+1)(1 - \mathrm{Re}\, S^J_{lja,lja}) \,. \tag{57}$$

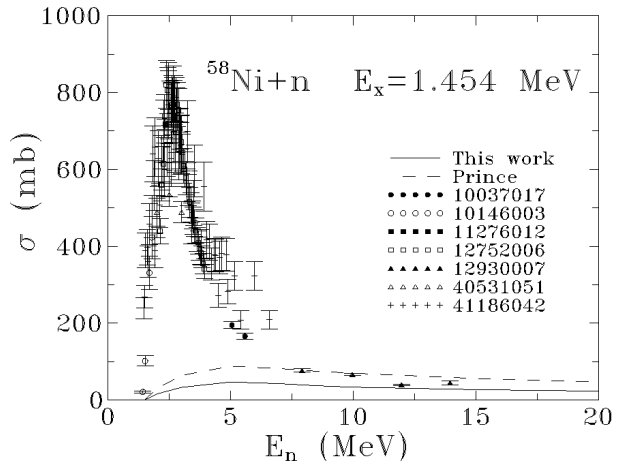

Figure 5: Various experimental measurements of the n+^{58}Ni E_x=1.454 MeV 2^+ inelastic cross section, identified by their EXFOR access numbers, are shown together with two optical model calculations.

The total cross section takes into account the occurence of scattering of any type. It is a measure of the flux lost from the incident plane wave state.

Just as in the case of the elastic cross section, care must be taken when comparing inelastic optical model cross sections with experimental data. At low energies, these cross sections are dominated by their compound nucleus contribution, as shown in Figs. 5 and 6, for neutron-induced excitation of the first excited state in ^{58}Ni and ^{238}U, respectively. One observes that the direct process plays a very minor role in the excitation of these states in the first few MeV above threshhold. In Fig. 5, the ^{58}Ni data are compared to optical model calculations using the parameters of A. Prince[19] and those of another set, both with a phonon amplitude of β_2=0.2. Note the strong influence of the optical model parameters on the direct component of the inelastic ^{58}Ni excitation. The Prince parameters yield an inelastic cross section that is almost twice that of the other set of parameters, although both use the same phonon amplitude. In Fig. 6, the ^{238}U data is compared to an optical model calculation using the parameters of Young and Arthur[22], which fits the higher energy data quite well. One notes that the direct excitation cross section of the ^{238}U 2^+ state reaches a value of almost 500 mb. In general, the inelastic excitation of a rotational band can be quite large, demanding a coupled channels method for its precise calculation.

The optical model and optical potential continue to be subjects of intense research. One can find out more about the directions this research is taking in the proceedings of a recent conference[23].

4 The Statistical Model

The statistical model describes the emission of the flux that is absorbed into the long-lived compound-nucleus states during a collision. The contribution of this flux to the average cross section is given by the average of the fluctuation term in the cross section, the second

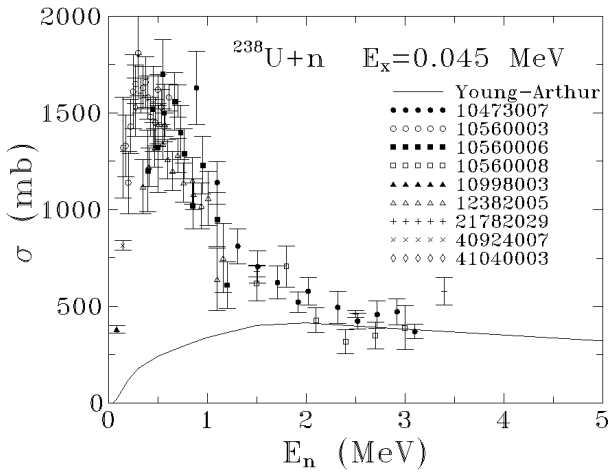

Figure 6: Various experimental measurements of the n+^{238}U E_x=0.044 MeV 2^+ inelastic cross section, identified by their EXFOR access numbers, are shown together with an optical model calculation.

term in the following expression,

$$\langle \sigma_{ac} \rangle = \frac{\pi}{k^2} \left| \bar{S}_{ca} - 1 \right|^2 + \frac{\pi}{k^2} \overline{|S_{fl,ca}|^2} \, .$$

Beginning with a convenient but general form of the S-matrix of Eq. (14), (the form given here has been simplified), one can use the observation that the amplitudes $g_{\mu c}$ and the matrix elements $V_{\mu\nu}$ coupling compound nuclear states (not included explicitly in Eq. (14)) can be treated, to a good approximation, as normally distributed random variables to calculate the average cross section explicitly. However, the calculation is extremely complex and requires sophisticated mathematical techniques for an exact resolution[24]. We will content ourselves here with simpler approximate solutions.

4.1 The Weisskopf-Ewing and Hauser-Feshbach models

The typical time scale for a direct reaction is of the order of 10^{-22} s while a low-energy compound nucleus reaction takes place on a time scale of 10^{-18} s or more. The extreme difference in the two time scales suggests that the formation and decay of the compound nucleus can be considered independent processes, with the decay ocurring from a configuration of equilibrium. Mathematically, this can be expressed as the factorization hypothesis, put forth by N. Bohr[25], which states that the compound nucleus cross sections can be written as the product of a factor describing the creation of the compound nucleus and a factor describing its decay. The symmetry in the corresponding factors, $g_{\mu a}$ and $g_{\mu c}$, of the resonance expansion S-matrix of Eq. (14) suggests that the creation and decay factors should have a similar form. One can thus postulate that compound nucleus cross sections may be written as

$$\sigma_{ac}^{fl} = \frac{\pi}{k_a^2} \xi_a \xi_c \, , \tag{58}$$

for an appropriate definition of the dimensionless quantity ξ_c. Summing over the decay channels of the compound nucleus, one obtains the total cross section for formation of the

compound nucleus, which will be used at the moment to define a factor Y_a that depends only on the entrance channel as

$$\frac{\pi}{k_a^2} Y_a = \sum_c \sigma_{ac}^{fl} .$$

Substituting in Eq. (58), one finds

$$Y_a = \xi_a \sum_b \xi_b \qquad \Rightarrow \qquad \sum_b Y_b = \left(\sum_b \xi_b \right)^2 ,$$

which immediately yields

$$\sigma_{ac}^{fl} = \frac{\pi}{k_a^2} \frac{Y_a Y_c}{\sum_b Y_b} = \frac{\pi}{k_a^2} Y_a \frac{Y_c}{\sum_b Y_b} . \tag{59}$$

In the last expression the fluctuation cross section has been written as the product of the formation cross section, $\pi Y_a / k_a^2$, and a branching ratio, $Y_c / \sum_b Y_b$. Both the independence of the formation and decay factors and the branching ratio form of the decay factor are characteristic of an equilibrated, statistical process.

To determine the absorption/emission factor Y_c, one now associates the compound nucleus formation cross section with the optical model absorption cross section. Two applications of this expression are widely used. These are the Weisskopf-Ewing and Hauser-Feshbach models of statistical emission.

In the Weisskopf-Ewing model[26], only energy, charge and mass conservation are taken into account. The quantity Y_c is then proportional to the absorption cross section summed (rather than averaged) over the projections of the projectile spin,

$$Y_c = (2s_c + 1) \frac{k_c^2}{\pi} \sigma_{abs}(E_c) = (2s_c + 1) \frac{2\mu_c}{\pi \hbar^2} E_c \sigma_{abs}(E_c) , \tag{60}$$

where μ_c is the reduced mass in channel c and E_c the center-of-mass energy in the channel. The cross section must be averaged over the projectile spin projections in the initial channel,

$$\sigma_{ac}^{fl} = \frac{1}{2s_a + 1} \frac{\pi}{k_a^2} \frac{Y_a Y_c}{\sum_b Y_b} . \tag{61}$$

In the Hauser-Feshbach model[27], angular momentum and parity conservation are taken into account as well. In this case, comparison with Eqs. (44) and (53) show that the quantity Y_c is a sum over the transmission coefficients that furnish the same total angular momentum J and parity π of the compound nucleus. When using spherical optical model transmission coefficients, the general expression for the absorption/emission factor is

$$Y_c(J, \pi) = \sum_{j=|J-I_c|}^{J+I_c} \sum_{l=|j-s_c|}^{j+s_c} f(l, \pi) \, T_l^j , \tag{62}$$

where $f(l, \pi)$ selects the correct values of the partial-wave parity and I_c is the angular momentum of the initial (final) nucleus before formation (after decay) of the compound nucleus. In the case of absorption/emission of a nucleon from a level with $I_c = 0$, this expression reduces to a single transmission coefficient. The cross section is obtained by

summing over all projections of the total angular momentum and averaging over the initial spins,

$$\sigma_{ac}^{fl} = \frac{1}{(2s_a+1)(2I_a+1)} \frac{\pi}{k_a^2} \sum_{J,\pi} (2J+1) \frac{Y_a(J,\pi)\, Y_c(J,\pi)}{\sum_b Y_b(J,\pi)} \,. \tag{63}$$

When using coupled-channels transmission coefficients, it is quite common to use just the diagonal elements of the transmission matrix and neglect the off-diagonal ones. An analysis by Engelbrecht and Weidenmüller [28] has shown that a more correct procedure is to perform the compound-nucleus calculation in a basis in which the transmission coefficients are diagonal and transform the resulting cross sections back to the non-diagonal basis

4.2 Further considerations

The factorization hypothesis assumes that no correlations exist between the formation and decay of the compound nucleus. In terms of the resonance expansion of the S-matrix, Eq. (14), this is equivalent to the hypothesis that the entrance channel amplitude $g_{\mu a}$ is uncorrelated with the exit channel amplitude, $g_{\mu c}$. This obviously cannot be the case for elastic scattering, in which the entrance and exit channels are identical. To take this correlation into account, a correction factor, known as a width fluctuation correction, is introduced into the Hauser-Feshbach partial wave cross section, which then takes the form,

$$\sigma_{ac}^{fl} = \frac{\pi}{k^2} (1 + (W_a - 1)\delta_{ac}) \frac{V_a\, V_c}{\sum_b V_b} \,.$$

The elastic enhancement factor, W_a, varies between 3, when the absorption is small ($T_a << 1$) and 2, when the absorption is strong ($T_a \approx 1$). The absorption/emission factors, Y_c, must be modified, when the width fluctuation correction is included, in order to preserve the relation between the summed fluctuation cross sections and the absorption cross section. This modification is denoted by the corrected absorption/emission factors V_c in the expression above. The width fluctuation correction leads to an elastic fluctuation cross section that is larger than the Hauser-Feshbach one, although not necessarily by a factor of 2 to 3, since the correction applies only to terms with exactly the same quantum numbers. The effect of the correction on other channels is most noticeable at low energies, in particular, at the threshold of the the first inelastic level, in cases where the only other open channel is γ emission. In this case, the corrected inelastic cross section lies below the Hauser-Feshbach one. Methods for estimating the width fluctuation correction may be found in Refs. [29, 30, 31, 32] and are discussed and compared in Ref. [33]. The method of Ref. [24] precludes such a correction by furnishing an exact expression for the cross section.

The emission factors Y_c in the Weisskopf-Ewing and Hauser-Feshbach expressions are required for all open channels. Taking neutron emission from a compound nucleus of total excitation energy E^*as an example, one need calculate the factor Y_c for each excited state of energy ε_c of the residual nucleus for which the neutron c.m. energy $E_n = E^* - \varepsilon_c - S_n$ is positive, S_n being the neutron separation energy. In practice, the ground state emission factor at the neutron energy E_n is usually used instead, ignoring any other differences between the ground and excited state emission factors.

At low excitation energies, individual states of a nucleus can be distinguished. However, state/level densities increase exponentially with the excitation energy, making their enumeration an impossible task at higher energies. Thus, above a set of discrete levels, one uses an emission factor weighted by the appropriate state/level density. For the Weisskopf-Ewing model,

$$Y_c(E^* - \varepsilon_c - S) \Longrightarrow Y_c(E^* - \varepsilon_c - S)\omega_c(\varepsilon_c)d\varepsilon_c\,, \tag{64}$$

where S is the separation energy and $\omega_c(\varepsilon_c)$ is the density of states of the residual nucleus at an energy of ε_c. Similarly, for the Hauser-Feshbach model,

$$Y_c(E^* - \varepsilon_c - S, J, \pi) \Longrightarrow Y_c(E^* - \varepsilon_c - S, J, \pi)\rho_c(\varepsilon_c, I_c)d\varepsilon_c\,, \tag{65}$$

where $\rho_c(\varepsilon_c, I_c)$ is the density of levels of the residual nucleus of angular momentum I_c at energy ε_c. As state and level densities vary quite rapidly with excitation energy, they play an extremely important role in statistical reactions and must be determined with care[34, 35].

Quite often, a compound nucleus, at the excitation energy under consideration, can emit more than one particle. When this is the case, the emissions are considered to be sequential and independent. It is then necessary to accumulate the distribution of residual nuclei when calculating the decay of each of the compound nuclei in the decay chain. It is usually necessary to calculate all possible paths in the chain. For example, a nucleus with one unit of charge and two units of mass less than the original compound nucleus can be populated by emission of a proton followed by a neutron, emission of a neutron followed by a proton or emission of a deuteron.

Finally it should be noted that compound nucleus angular distributions may also be calculated. In general, they are not isotropic, since angular momentum is conserved. However, they are symmetric about 90^o, reflecting the loss of memory of the initial momentum.

5 Preequilibrium models

Up to this point, nuclear reactions have been considered to occur on two distinct time scales. This point of view is valid at low energies, but becomes less so as the incident energy increases. Due to the two-body nature of the nuclear interaction, a nucleon-nucleus interaction may be decomposed as a series of nucleon-nucleon interactions. Taking the entrance channel of a nucleon-nucleus composite system to be a 1 (projectile) particle, 0 (target) hole state, one can consider the result of a collision as leading to either another 1p-0h state or to a set of 2p-1h states, in each of which the incident particle has excited one of the target particles, creating a particle-hole pair. At energies up to about 20 to 30 MeV, the wavelength of a nucleon is still about 5 to 6 fm, so that the projectile nucleon - target nucleus interaction would not excite an individual particle-hole state, but a complicated linear combination of particle-hole states. Further interaction of any of the particles or holes could create, scatter or destroy such particle-hole pair configurations. But in all cases, one can classify the complex configurations in terms of the number of particles p and number of holes h. One notes that, since the total number of particles is conserved, the difference between the number of particles and number of holes, $p - h$, remains constant throughout a collision.

The quantity $n = p + h$, called the exciton number, thus serves as an unambiguous label of the configuration of the system within this picture (see, however, Ref. [36]).

At low energy, where the lifetime of the compound nucleus is long (that is, the emission rates are small), one expects the compound system to usually reach equilibrium before decaying. As the incident energy increases, emission rates increase as well, and the likelihood of preequilibrium particle emission increases. As the preequilibrium configurations do not share the excitation energy among as many degrees of freedom as the equilibrium ones do, particles emitted from preequilibrium configurations tend to have more energy than those emitted from equilibrium. They may also preserve some memory of the direction of the incident nucleon, resulting in forward peaked angular distributions.

One may use the exciton picture to refine the decomposition of the space of states into a prompt component P and a compound nucleus component Q, Eq. (2), as

$$P = P_1 + P_3 + P_5 + P_7 + \dots , \tag{66}$$

$$Q = Q_3 + Q_5 + Q_7 + \dots . \tag{67}$$

The decomposition of the direct reaction space P contains the elastic component P_1 and a series of components with increasing exciton number in which it is assumed that one (and only one) of the nucleons continues in the continuum. Progression along the stages of the P chain could result either from additional interactions of the continuum nucleon with the target or from interactions within the target. The decomposition of the compound nucleus space begins with the three-exciton configuration Q_3, since the incident nucleon must collide with at least one nucleon, forming a two-particle, one-hole configuration, in order to be captured into a quasi-bound state. Transitions between the chains may also occur at any stage. However, it is assumed that all transitions change the exciton number by at most two.

Reactions that occur in the direct reaction space P are known as multistep direct reactions. Those that occur in the compound nuclear space Q are known as multistep compound reactions. The first multistep direct models were developed by Feshbach, Kerman and Koonin[37] and by Tamura, Udagawa and Lenske[38] and later by Nishioka, Weidenmüller, and Yoshida[39]. The first multistep compound model was developed by Agassi, Weidenmüller and Mantzouranis[40] and redeveloped using more rigorous methods in Ref. [42]. Similar models were also proposed in Refs.[37] and [41]. Before discussing the multistep models, however, it is worthwhile examining the original 'classical' exciton model, which bears a very strong resemblance to the later multistep compound model.

5.1 The exciton model

The exciton model was originally proposed by Griffin[43] and later cast in the form of a time-dependent master equation by Cline and Blann[44]. In their formulation, energy is conserved, but angular momentum is not. The equation governing the time development of the fraction of the cross section $P(n)$ in the n exciton configuration is written as

$$\frac{dP(n)}{dt} = \lambda_-(n+2)\,P(n+2) + \lambda_0(n)\,P(n) + \lambda_+(n-2)\,P(n-2) - \lambda(n)\,P(n) \tag{68}$$

where $\lambda(n)$ is the total rate of transitions out of the n exciton configuration,

$$\lambda(n) = \lambda_-(n) + \lambda_0(n) + \lambda_+(n) + \lambda_e(n),$$

with $\lambda_e(n)$ being the total rate of particle emission from the n exciton configuration. The quantities $\lambda_-(n)$, $\lambda_0(n)$, and $\lambda_+(n)$ are the average rates for internal transitions from the n exciton configuration with a change of exciton number by -2, 0, or +2. The average rate of transitions that do not change the number of excitons cancels exactly in this simple formulation of the model, but not in more general models. Although the transition rates are labeled by the exciton number n, for brevity, they in fact depend on the particle and hole numbers, p and h, as well as the total excitation energy E. Since the energy and the difference between the particle and hole numbers, $p - h$, are conserved, no ambiguity is introduced by this simplification.

Using Fermi's golden rule, the internal transition rates can, in principal, be calculated by summing over all squared residual interaction matrix elements leading from the initial to the final configuration. In practice, this sum is written as the product of the average squared matrix element of the residual interaction $|M|^2$with the density of available states. One has, for the transitions that change the exciton number by two,

$$\begin{aligned}
\omega(n,E)\,\lambda_+(n) &= \omega(n+2,E)\,\lambda_-(n+2) \\
&= \frac{|M|^2}{h}\int_0^E d\varepsilon\,(\omega(2,1,\varepsilon)\omega(1,0,\varepsilon)\omega(p-1,h,E-\varepsilon) \\
&\qquad +\omega(1,2,\varepsilon)\omega(0,1,\varepsilon)\omega(p,h-1,E-\varepsilon)), \\
&\equiv \pi_{n,n+2}(E)
\end{aligned} \tag{69}$$

while for the transitions preserving the exciton number,

$$\begin{aligned}
\omega(n,E)\,\lambda_0(n) &= \frac{|M|^2}{h}\int_0^E d\varepsilon\,(\omega(2,0,\varepsilon)\omega(2,0,\varepsilon)\omega(p-2,h,E-\varepsilon) \\
&\qquad +\omega(1,1,\varepsilon)\omega(1,1,\varepsilon)\omega(p-1,h-1,E-\varepsilon) \\
&\qquad +\omega(0,2,\varepsilon)\omega(0,2,\varepsilon)\omega(p,h-2,E-\varepsilon)). \\
&\equiv \pi_{n,n}(E)
\end{aligned} \tag{70}$$

In each case, the ratio of the integral on the right hand side with the density of states on the left hand side furnishes the density of available states. For the exciton number changing transitions, the density of available states counts the average number of ways by which any single exciton of the initial particle-hole configuration can be converted to three excitons (or vice versa), assuming the energy-conserving transition between any of the single exciton states and any of the three-exciton states to occur with equal likelihood. Similarly, the density of available states for transitions that do not change the exciton number counts the average number of ways in which any two excitons may scatter from one another, again assuming equal likelihood for all energy-conserving transitions. Expressions for the density of available states were given by Williams[45] and later corrected for the Pauli principle by Cline[46].

Although several different expression for the average matrix element, $|M|^2$, are in use, the most common one is that proposed by Kalbach-Cline[47],

$$|M|^2 = \frac{f_M}{A^3 E},$$

where A is the mass number of the system and f_M is a parameter, which is usually taken to be about $f_M = 230$ MeV^3 .

The particle emission rate $\lambda_e(n)$ in the simple exciton model is the sum of the integrated proton and neutron differential emission rates, $\frac{d\lambda_{e\nu}}{d\varepsilon_\nu}(n,\varepsilon_\nu)\,d\varepsilon_\nu$, which can be written in terms of the Weisskopf-Ewing emission factors of Eq. (60) (no angular momentum conservation), as[44, 48]

$$\begin{aligned}\frac{d\lambda_{e\nu}}{d\varepsilon_\nu}(n,\varepsilon_\nu)\,d\varepsilon_\nu &\equiv \frac{Y_\nu(n)R_\nu}{h\,\omega(n,E)} \\ &= \frac{(2s_\nu+1)}{\pi^2\hbar^3}\mu_\nu\,\varepsilon_\nu\,\sigma_\nu(\varepsilon_\nu)\,R_\nu\frac{\omega(p-1,h,E-B_\nu-\varepsilon_\nu)}{\omega(p,h,E)}\,d\varepsilon_\nu, \qquad (71)\end{aligned}$$

where μ_ν is the reduced mass of the emitted neutron/proton, ε_ν its outgoing kinetic energy, B_ν its separation energy, and $\sigma_\nu(\varepsilon_\nu)$ the cross section for the inverse absorption process. The factor $Y_\nu(n)$ denotes the generalization of the expression in Eq. (64) to the case in which the residue density of states is an exciton one. A factor R_ν is also included to take into account the fact that neutrons and protons have not been distinguished in the process. Emission of more composite particles, such as alphas, may also be taken into account by taking the factor R_ν as an exciton-number-dependent probability for striking the preformed composite[49] and by modifying the density of final states accordingly.

The densities of states are often taken to be the Williams densities[50],

$$\omega(p,h,E) = \frac{g\;(gE - A_{p,h})^{p+h-1}}{p!\,h!\,(p+h-1)!},$$

where the Pauli blocking correction $A_{p,h}$ is given by

$$A_{p,h} = \frac{1}{4}\left(p^2 + h^2 + p - 3h\right).$$

These densities are obtained by counting all configurations consistent with the Pauli principle having a total energy E, assuming an equally-spaced set of single particle states. The parameter g is the single-particle state density, which is usually taken to be $g = \frac{6}{\pi^2}a$, with a the level density parameter. The differential emission rates differ from the usual Weisskopf-Ewing compound nucleus emission ones only in the factor R_ν and in the use of exciton state densities rather than compound nucleus ones.

The time evolution equations, Eq. (68), form a set of coupled linear differential equations, whose solution may be written in the form of a vector as,

$$\vec{P}(t) = \exp\left[-\Lambda^{-1}\,t\right]\;\vec{P}_{0,}$$

where the matrix Λ^{-1} is given by

$$\left(\Lambda^{-1}\right)_{nm} = \lambda(n)\,\delta_{m,n} - \lambda_{-}(n+2)\,\delta_{m,n+2} - \lambda_0(n)\,\delta_{m,n} - \lambda_{+}(n-2)\,\delta_{m,n-2},$$

and the vector $\vec{P}_0$ describing the initial exciton configuration of the system is usually taken to be,

$$P_0(n) = \sigma_0 \delta_{p,p_0} \delta_{h,h_0},$$

where σ_0 is the spin-averaged absorption cross section, proportional to the spin-averaged Weisskopf-Ewing absorption factor of Eq. (60) and consistent with the the neglect of angular momentum. In the case of nucleon-induced reactions, the initial configuration is the two particle, one hole one.

The differential and total emission cross sections may be obtained by integrating the emission rates over all time,

$$\frac{d\sigma_\nu}{d\varepsilon_\nu}(\varepsilon_\nu) = \sum_n \int_0^\infty \frac{d\lambda_{e\nu}}{d\varepsilon_\nu}(n,\varepsilon_\nu)\,P(n,t)\,dt = \sum_{n,m} \frac{d\lambda_{e\nu}}{d\varepsilon_\nu}(n,\varepsilon_\nu)\,\Lambda_{n,m} P_0(m).$$

It is interesting to rewrite this in a form more similar to the Weiskopf-Ewing expression for the statistical emission cross section, Eq. (61). To do this, one removes the factor of h and the density of states $\omega(n,E)$ from the denominator of the emission rate, Eq. (71), passing them to the matrix Λ, resulting in

$$\frac{d\sigma_\nu}{d\varepsilon_\nu}(\varepsilon_\nu) \equiv \sigma_{0\nu} = \frac{1}{2s_0+1} \sum_{n,m} R_\nu Y_\nu(n)\,\Pi_{n,m} Y_0(m), \tag{72}$$

where

$$\left(\Pi^{-1}\right)_{nm} = 2\pi\omega(n,E)\Gamma_n\,\delta_{m,n} - \pi_{n,n+2}\,\delta_{m,n+2} - \pi_{n,n}\,\delta_{m,n} - \pi_{n,n-2}\,\delta_{m,n-2}, \tag{73}$$

where the $\pi_{n,m}$ are given in Eqs. (69) and (70) and

$$2\pi\omega(n,E)\,\Gamma_n = \pi_{n,n+2} + \pi_{n,n} + \pi_{n,n-2} + \sum_c R_c Y_c(n). \tag{74}$$

When the emission factors $Y_c(n)$ are very small compared to the internal transition factors $\pi_{n,n\pm2}$ and $\pi_{n,n}$, the smallest eigenvalue of the matrix Π approaches $\sum_{c,n} R_c Y_c(n)$. The corresponding eigenvector is $(1,1,1,...)$, corresponding to equal occupation of all configurations. The cross section then reduces to

$$\sigma_{0\nu} = \frac{1}{2s_0+1} \frac{\sum_n R_\nu Y_\nu(n)\ \sum_m Y_0(m)}{\sum_{c,n} R_\nu Y_c(n)}.$$

When the sum over the exciton state densities reproduces the total density of states, this expression is equal to the Weisskopf-Ewing expression for statistical decay of Eq. (61), with the exception of the factor R_ν. The equilibrium limit of statistical emission is thus contained in the exciton model.

The exciton model has been generalized to include angular momentum[51] and to distinguish between protons and neutrons[52, 53, 54]. Both generalizations are fairly straighforward. The generalization including angular momentum requires that the densities of states be replaced by angular-momentum dependent level densities and that the Weisskopf-Ewing emission factors be replaced by the corresponding Hauser-Feshbach ones of Eqs. (62) and (65). The transition rates have the same form as those in Eqs. (69) and (70), but with the densities of states replaced by level densities and the average matrix elements by the appropriate average reduced matrix elements.

The generalization of the exciton model to distinguish between protons and neutrons requires that one use densities of states (or levels) that distinguish between proton and neutron particles and holes. The number of transition rates increases greatly in this case because of the number of different types of transitions that must be distinguished but, again, may be written in a form similar to those of Eqs. (69) and (70). The transition rates that do not change the total exciton number no longer cancel here, due to transitions between proton and neutron particle-hole pairs. Both generalizations lead to better agreement of the exciton model calculations with the experimental data.

Much work has been done to generalize the exciton model to permit its use in calculating angular distributions, as well as spectra[51, 55, 56, 57, 58, 59]. Due to lack of space and time, these cannot be discussed here.

5.2 The multistep compound model

The exciton model does not distinguish between bound and unbound single-particle states. One of the principal differences between this model and the multistep compound one is that the multistep compound model does make this distinction and includes in its state/level densities only those states/levels in which all of the single-particle states are bound. One can thus obtain a multistep compound model by taking the expressions above for the exciton model, Eqs. (69) and (70) defining the transition rates and Eqs. (74), (73), and (72) defining the exciton configuration widths, the transition matrix and the cross sections, respectively, and substituting state/level densities which include only bound single-particle states[60, 61].

The other principal difference between the exciton model and the multistep compound one is that the latter requires an interaction to occur for a nucleon to be absorbed or emitted from the composite system. In the case of an emission factor, the transition must raise one of the nucleons to an unbound, continuum state, so that it can leave the system. In the case of an absorption factor, the transition must lower the initially unbound nucleon to a bound configuration. These factors may be obtained in analogy with the internal transition factors of Eqs. (69) and (70) as

$$Y_{c+}(n) = |M_c|^2 \int_{\varepsilon_c}^{E} d\varepsilon\, \omega(0,2,\varepsilon-\varepsilon_c)\omega(0,1,\varepsilon)\omega(p,h-1,E-\varepsilon))\,,$$

$$\begin{aligned} Y_{c0}(n) &= |M_c|^2 \int_{\varepsilon_c}^{E} d\varepsilon\, (\omega(1,0,\varepsilon-\varepsilon_c)\omega(2,0,\varepsilon)\omega(p-2,h,E-\varepsilon) \\ &\quad +\omega(0,1,\varepsilon-\varepsilon_c)\omega(1,1,\varepsilon)\omega(p-1,h-1,E-\varepsilon))\,, \end{aligned}$$

and

$$\begin{aligned} Y_{c-}(n) &= |M_c|^2 \int_{\varepsilon_c}^{E} d\varepsilon\, \omega(0,0,\varepsilon-\varepsilon_c)\omega(2,1,\varepsilon)\omega(p-2,h-1,E-\varepsilon) \\ &= |M_c|^2 \omega(2,1,\varepsilon_c)\omega(p-2,h-1,E-\varepsilon_c). \end{aligned}$$

Note that the one-particle to two-particle, one-hole transitions cannot contribute to $Y_{c+}(n)$ because of the restriction to bound state configurations. The emission factors in Eqs. (74), (73), and (72) defining the exciton configuration widths, the transition matrix and the cross sections, respectively, are then

$$Y_c(n) = Y_{c+}(n) + Y_{c0}(n) + Y_{c-}(n)\,.$$

The absorption factors describe the inverse process to emission and may be obtained by reinterpreting the above expressions. In particular, the absorption factor for creating the initial $2p-1h$ configuration is $Y_{0-}(3) = |M_0|^2\omega(2,1,\varepsilon_0)$. The coefficients $|M_c|^2$ may be determined by adjusting the sum $\sum_n Y_c(n)$ to the absorption cross section times the final state/level density or by fitting the cross section. The multistep compound emission/absorption factors were first derived in Ref. [37]. Explicit expressions for them and a general discussion of multistep compound processes may be found in Ref. [62].

A nucleon that undergoes a transition to the continuum can return to a bound-state configuration due to another transition before escaping the nucleus. This introduces an additional component, proportional to the product of an emission and an absorption factor, in the multistep compound transition matrix, Eq. (73). This term, called the external mixing component, permits transitions (through the continuum) that change the exciton number by up to 4. It is derived and discussed in Ref. [40], but is usually not included in actual multistep compound calculations.

Although it was not done here, the expressions for the multistep compound model can be obtained using the decomposition of the space of states into the chains of prompt and compound nucleus exciton configurations given in Eq. (67). One manner to derive these expressions is to assume the ensembles of individual interactions coupling the prompt configurations to the compound ones and the compound ones among themselves to be independent random variables. Approximate evaluations of the multistep process based on these assumptions may be found in Refs. [40] and [37] and a much more rigorous, but mathematically sophisticated, derivation in Ref. [42].

5.3 The multistep direct model

To obtain expressions for multistep direct reactions, one again uses the decomposition of the space of states into the chains of prompt and compound nucleus exciton configurations. In this case, one must analyze the coupling along the chain of prompt configurations and, of course, their coupling to the compound nucleus states. One again assumes the ensemble of interactions coupling the prompt configurations among themselves and those coupling the prompt configurations to the compound nucleus states to be independent random variables, when evaluating the contributions to the cross sections.

When the generalized optical model was discussed earlier, the scattering amplitude was assumed to have been obtained from a direct solution of the coupled-channels equations. This is indeed the best method for calculating the cross sections of strongly coupled levels. In general, however, only very few levels are strongly coupled. The excitations of the multistep direct model, in particular, are assumed to be individually weak, but large in number. In this case, it is advantageous to rewrite the Schrödinger equation as a Lippmann-Schwinger equation,

$$(E - H_0 - V)|\psi >= 0 \quad \longrightarrow \quad |\psi >= |\phi > + \frac{1}{E - H_0} V|\psi >,$$

where $(E - H_0)|\phi >= 0$, and approximate the wavefunction $|\psi >$ using back-substitution on the right-hand side.

For the analysis of multistep direct reactions, the most convenient form of the Hamiltonian is one in which the interaction V is decomposed into a set of spherical optical potentials V_{0n}, with V_{0n} common to the states of the n-exciton configuration, and a set of two-body interactions v that couple the states in different configurations. The set of interactions that couple states within an exciton configuration are neglected here. The set of spherical optical potentials V_0 is then placed in the unperturbed hamiltonian H_0, leaving only the interactions v to couples configurations in the right-hand term of the Lippmann-Schwinger equation. With the appropriate incoming-wave boundary conditions on the wave functions, the Lippmann-Schwinger equation then becomes

$$|\psi^{(+)} >= |\phi_i^{(+)} > + g^{(+)}(E')v|\psi^{(+)} >,$$

where $g^{(+)}(E') = (E' - H_0 - V_0 + i\eta)^{-1}$ is the Green's function with an outgoing-wave boundary condition, evaluated at an energy consistent with the gain or loss of energy in the collision. Back-substituting in the second term on the right-hand side and explicitly labelling the exciton configurations yields

$$\begin{aligned} |\psi^{(+)} > \;\; = \;\; & |\phi_i^{(+)} > + g_3^{(+)}(E_3)v_{31}|\phi_i^{(+)} > + g_5^{(+)}(E_5)v_{53}g_3^{(+)}(E_3)v_{31}|\phi_i^{(+)} > \\ & + g_1^{(+)}(E)v_{13}g_3^{(+)}(E_3)v_{31}|\phi_i^{(+)} > + \cdots, \end{aligned}$$

where sums over all intermediate states (E_3 in the two-step amplitudes) and final states (E_3 in the one-step amplitudes and E_5 in the two-step amplitudes) have been left implicit.

The terms on the first line of the above expression show the progression of the initial flux through the states of higher and higher exciton configurations. The term on the second line describes flux that has been excited to the states of the 3-exciton configuration and then transferred back to the 1-exciton state. This term is a correction to the 1-exciton wave function that takes into account the flux that has been lost to the states of the 3-exciton configuration. It will be neglected here, as is done in most numerical calculations of multistep direct reactions.

To calculate cross sections, one must now extract the scattering amplitudes from the asymptotic behavior of the components of the wave function, square them and sum over all intermediate and (some) final states. For the one- and two-step processes above, one finds for the scattering amplitudes,

$$\begin{aligned} f_3(E, \Omega \leftarrow E_i, \Omega_i) \;\; &= \;\; < \phi_{3f}^{(-)}(E)|v_{31}|\phi_i^{(+)} > \\ f_5(E, \Omega \leftarrow E_3 \leftarrow E_i, \Omega_i) \;\; &= \;\; < \phi_{5f}^{(-)}(E)|v_{53}g_3^{(+)}(E_3)v_{31}|\phi_i^{(+)} > \; . \end{aligned}$$

where the $< \phi^{(-)}|$ are solutions to the spherical optical Hamiltonian with outgoing wave boundary conditions. Using the same simplifying approximations used in the exciton and multistep compound models, these furnish average cross sections of the form

$$\begin{aligned}
\frac{d^2\sigma^{(3)}(E,\Omega \leftarrow E_i,\Omega_i)}{d\Omega dE} &= \frac{m^2}{(2\pi\hbar^2)^2}\frac{k}{k_i}\omega(1,1,E_i-E)\left|< \phi_{3f}^{(-)}(E)|\bar{v}_{31}|\phi_i^{(+)} >\right|^2 , \\
\frac{d^2\sigma^{(5)}(E,\Omega \leftarrow E_i,\Omega_i)}{d\Omega dE} &= \frac{2m^5}{(2\pi)^5\hbar^{10}}\frac{k}{k_i}2\pi^2\int dE_3\,\omega(1,1,E_3-E)\,\omega(1,1,E_i-E_3)\times \\
&\qquad \times\left|< \phi_{5f}^{(-)}(E)|\bar{v}_{53}g_3^{(+)}(E_3)\bar{v}_{31}|\phi_i^{(+)} >\right|^2 ,
\end{aligned}$$

where $\omega(1,1,E_x)$ is the 1p-1h density of states at energy E_x and $\bar{v}$ is an average residual interaction. The one-step cross section leading to the three exciton configuration does not require the hypothesis that the matrix elements are statistically independent, as it is a simple sum of cross sections. The statistical hypothesis has been used to obtain the two-step cross section to the five exciton configuration in order to reduce the coherent intermediate sum of the amplitudes to an incoherent one. If the energy dependence of the intermediate propagator $g^{(+)}(E_3)$ in the two-step cross section is taken at a some average value, the remaining convolution of densities leads to the density of available 2p-2h states, analogous to the result one would expect from the exciton or multistep compound model.

Tamura, Udagawa and Lenske [38] performed some of the first multistep direct calculations using forms of the cross sections similar to those above. They, however, did not use an average residual interaction together with simple exciton configuration densities. Instead, they calculated a 1p-1h response function by diagonalizing the target nucleus Hamiltonian in the 1p-1h subspace. They then convoluted the 1p-1h response with itself to obtain the 2p-2h response function.

Feshbach, Kerman and Koonin argued instead that the two-cross section could be reduced to a convolution of one-step ones[37],

$$\begin{aligned}
\frac{d^2\sigma^{(5)}(E,\Omega \leftarrow E_i,\Omega_i)}{d\Omega dE} &= \frac{m}{4\pi^2\hbar^2}\int d\Omega_1\int dE_1\frac{d^2\sigma^{(3)}(E,\Omega \leftarrow E_1,\Omega_1)}{d\Omega dE} \\
&\qquad \times E_1\frac{d^2\sigma^{(3)}(E_1,\Omega_1 \leftarrow E_i,\Omega_i)}{d\Omega_1 dE_1} .
\end{aligned} \tag{75}$$

The simplicity of this expression and the facility with which it may be extended to higher numbers of interactions has made it a popular form of the multistep direct reaction theory. Although there still exists some controversy over the validity of the approximation, it has been widely used and has usually shown good agreement with experimental data[64, 65].

As the density of 1p-1h and 2p-2h states is fairly sparse, it is feasible to perform microscopic multistep direct calculations that explicitly include all states. By distinguishing protons and neutrons, it is also possible to include charge exchange as well as inelastic transitions in the multistep direct cascade. Both of these have been done in Ref. [65] and result in a generally excellent agreement with the experimental data.

Finally, it should be noted that the intermediate stages in the multistep direct chain can also feed the multistep compound process. As such transitions enter the multistep compound

chain at a higher exciton number than those that enter it directly from the nuclear ground state, they tend to decrease the multistep compound preequilibrium emission rather than increase it. Most preequilibrium multistep compound emissions come from the first few stages in the chain. A composite system formed with a higher exciton number has a greater chance of evolving to equilibrium before decaying than one formed with a smaller exciton number.

6 The intranuclear cascade model

The statistical equilibrium and preequilibrium models discussed up to this point assume that all the states collected in a configuration, be it an exciton one or the entire compound nucleus, are somehow mixed with one another so that their energy is distributed statistically. Although this appears to be a good approximation at low energies, it certainly does not remain so as the energy increases. At sufficiently high energies, the velocity of an incident nucleon can be over four times that of the fastest nucleon in the nucleus. In such cases, models that go to the other extreme and assume no configuration mixing at all become relevant. Among models of this type are the intranuclear cascade model[66, 67, 68, 69], as well as the hybrid model[70, 71, 72] and the hybrid Monte-Carlo simulation[73, 74] of M. Blann. Here, the intranuclear cascade model and the hybrid Monte-Carlo simulation will be discussed.

6.1 The intranuclear cascade model

The intranuclear cascade model uses the Monte Carlo method to simulate a nuclear reaction. A typical calculation assumes the target to initially be a cold Fermi gas of nucleons in a potential well. All hadrons (nucleons and pions) move classically according to the average mean nuclear potential. The interaction probability per unit length for a particle is taken to be the inverse of its mean free path, averaged over the Fermi motion of the target nucleons. Interactions occur as in the center-of-mass system of the two particles in free space. Interactions are incoherent and uncorrelated. Pauli blocking is usually included. All particles that have interacted are treated exactly the same, their trajectories being followed and their chances for interacting calculated.

In a typical calculation, once the geometrical parameters have been defined, the primary nucleon is propagated into the nucleus, its probability for having interacted calculated at each step. When an interaction occurs, the momentum of the primary particle changes, together with that of the secondary. Usually, the primary nucleon is followed until it leaves the nucleus. The secondaries are then followed and allowed to interact, each in its turn, until they either leave the nucleus or loses sufficient energy to become bound again. When all particle energies are below a particular level, a preequilibrium stage may be substituted for the intranuclear cascade. When all remaining particles are bound (or nearly so), a Weisskopf-Ewing statistical model is used to calculate further emissions and activation cross sections.

The intranuclear cascade model shows reasonably good agreement with the experimental data, except at energies below about 100 MeV. The model describes nucleon and pion

emission fairly well but does not provide as reliable a description of activation cross sections. It also cannot describe cluster emission (such as alpha emission). Little by little, however, improvements are being made in the model and the agreement between its calculations and the experimental data is growing. A detailed discussion of the model and its possibilities may be found in Ref. [69].

6.2 The hybrid Monte Carlo simulation

The hybrid Monte-Carlo simulation uses the Monte Carlo method to simulate a nuclear reaction in the energy space of exciton configurations, rather than in geometrical space as does the intranuclear cascade model. It treats only the 2p-1h configurations, which have been shown to be a good approximation to the distribution that results from a nucleon-nucleon collision in nuclear matter[75]. For each particle in a 2p-1h configuration, an energy above the Fermi energy is attributed randomly. If the particle energy is above the binding energy, it may either escape or rescatter to form another 2p-1h pair, which it again does randomly. If it escapes, the remaining energy of the 1p-1h pair is divided randomly between the particle and the hole and the new particle is tested for escape or rescattering. This goes on until all particles are bound. Hole scatterings are then considered and are also found to contribute to the particle emission. The hybrid Monte-Carlo model can also calculate angular distributions[74].

7 Final remarks

These notes have tried to sketch several standard models used to describe nucleon-induced reactions. Only the most basic applications are addressed and, even then, only in their simplest form. Because of these limitations, the contributions of many resarchers have not been recognized. The views and conclusions of others have no doubt been distorted and misrepresented. The author offers his apologies to all.

Acknowledgments

The author would like to thank the organizers for this opportunity to offer his views on this vast subject. He also acknowledges partial support provided by the Brazilian National Research Council (CNPq), grant 303131/2021-7, and by the São Paulo Research Foundation (FAPESP), grant 2017/05660-0.

References

[1] C.M. Perey, F.G. Perey, J.A. Harvey, N.W. Hill, N.M. Larson, R.L. Macklin,"^{58}Ni+n transmission, differential elastic scattering and capture measurements and analysis from 5 to 813 keV", ORNL-TM-10841, (1988); EYFOR file #12972003.

[2] H. Feshbach, *Theoretical Nuclear Physics: Nuclear Reactions*, John Wiley and Sons, Inc., New York (1992).

[3] F.H. Fröhner, in *Proceedings of the Workshop on Nuclear Reaction Data and Nuclear Reactors: Physics, Design and Safety* (1996), World Scientific, Singapore, (1998), p.54.

[4] N.M. Larson, in *Proceedings of the Workshop on Nuclear Reaction Data and Nuclear Reactors: Physics, Design and Safety* (1998), World Scientific, Singapore, (1999), p.1.

[5] A. Brusegan, G.Rohr, R.Shelley, E.Macavero, C. Van Der Vorst, F. Poortmans, I. Mewissen, and G. Vanpraet, "Very high resolution transmission measurements and resonance parameters of ^{58}Ni and ^{60}Ni"; EXFOR file #22314006.

[6] T.Ericson, Advances in Physics, Vol. IX, No. 36, 425 (1960).

[7] J.P. Delaroche, Ch. Lagrange, and J. Salvy, IAEA-190, Vol. 1, (Vienna, 1976), p. 251.

[8] J.P. Jeukenne, A. Lejeune, and C. Mahaux, Phys. Rev. **C16**, 80 (1977).

[9] C. Mahaux and R. Sartor, in *Proceedings of the Specialists' Meeting on the Use of the Optical Model for the Calculation of Neutron Cross Sections below 20 MeV*, OECD, Paris, (1986), p. 17.

[10] F. Osterfeld, in *Proceedings of the Specialists' Meeting on the Use of the Optical Model for the Calculation of Neutron Cross Sections below 20 MeV*, OECD, Paris, (1986), p. 29.

[11] K. Amos, P.J. Dortmans, H.V. von Geramb, S. Karataglidis, and J. Raynal, Adv. in Nucl. Phys. **25**, 276 (2000).

[12] B.D. Serot and J.D. Walecka, Adv. Nucl. Phys. **16** 1 (1986).

[13] R.J. Glauber, in *Lectures in Theoretical Physics*, Interscience, New York, (1959), Vol. 1, p. 315.

[14] A.K. Kerman, H. McManus, and R.M. Thaler, Ann. Phys. (N.Y.) **8**, 551 (1959).

[15] C. Mahaux and H. Ngô, Nucl. Phys. **A378**, 205 (1982).

[16] C. M. Perey and F. C. Perey, Nucl. Dat. Tab. **14**, 293 (1974).

[17] *Handbook for calculations of nuclear reaction data : Reference input parameter library*, IEAE-TECDOC-1034; See also http://www-nds.iaea.or.at.

[18] R. G. Newton, *Scattering Theory of Waves and Particles*, McGraw-Hill, Inc., New York (1966).

[19] A. Prince, in *Proceedings of the International Conference on Nuclear Data*, Antwerp, (1982).

[20] A. deShalit and H. Feshbach, *Theoretical Nuclear Physics Volume 1: Nuclear Structure*, John Wiley and Sons, Inc., New York (1974).

[21] G.R. Satchler, Phys. Lett. B **36**, 55 (1963).

[22] P.G. Young, in *Handbook for calculations of nuclear reaction data: Reference input parameter library*, IEAE-TECDOC-1034, p.131.

[23] *Proceedings of the Specialists' Meeting on the Nucleon Nucleus Optical Model up to 200 MeV*, OECD, Bruyères-le-Chatel (1996).

[24] J.J.M. Verbaarschot, H.A. Weidenmüller, and M.R. Zirnbauer, Phys. Rep. **129**, 367 (1985).

[25] N. Bohr, Nature **137**, 344 (1936).

[26] V.F. Weisskopf and D.H. Ewing, Phys. Rev. **57**, 472, 935 (1940).

[27] W. Hauser and H. Feshbach, Phys. Rev. **87**, 366 (1952).

[28] C.A. Engelbrecht and H.A. Weidenmüller, Phys. Rev. **C8**, 859 (1973).

[29] P.A. Moldauer, Phys. Rev. **C11**, B642 (1974).

[30] P.A. Moldauer, Nucl. Phys. A **344**, 185 (1980).

[31] H.M. Hofmann, J. Richert, J.W. Tepel, and H.A. Weidenmüller, Phys. Lett. B **49**, 1 (1974).

[32] H.M. Hofmann, T. Mertelmeier, M. Herman, and J.W. Tepel, Z. Phys. A **297**, 153 (1980).

[33] M. Herman, in *Proceedings of the Workshop on Nuclear Reaction Data and Nuclear Reactors: Physics, Design and Safety* (1998), World Scientific, Singapore, (1999), p.121.

[34] A. Gilbert and A.G.W. Cameron, Can. J.Phys. **43**, 1446 (1965).

[35] A.V. Ignatyuk,G.N. Smienkin, and A.S. Tishin, Sov. J. Nucl. Phys. **21**, 255 (1975).

[36] J. Bisplinghoff, Phys. Rev. **C33**, 1569 (1986).

[37] H. Feshbach, A. Kerman, and S. Koonin, Ann. Phys. (N.Y.) **125**, 429 (1980).

[38] T. Tamura, T. Udagawa, and H. Lenske, Phys. Rev. **C26**, 379 (1982).

[39] H. Nishioka, H.A. Weidenmüller, and S. Yoshida, Ann. Phys. (NY) **183**, 166 (1988).

[40] D. Agassi, H.A. Weidenmüller, and G. Mantzouranis, Phys. Rep. **22**, 145 (1975).

[41] W.A. Friedman, M.S. Hussein, K.W. McVoy, and P. Mello, Phys. Rep. **77**, 47 (1981); K.W. McVoy and X.T. Tang, Phys. Rep. **94**, 139 (1983).

[42] H. Nishioka, J.J.M. Verbaarschot, H.A. Weidenmüller, and S. Yoshida, Ann. Phys. (NY) **172**, 67 (1986).

[43] J.J. Griffin, Phys. Lett. **17**, 478 (1966).

[44] C.K. Cline and M. Blann, Nucl. Phys. **A172**, 225 (1972).

[45] F.C. Williams Jr., Phys. Lett. B **31**, 184 (1970).

[46] C.K. Cline, Nucl. Phys. **A195**, 353 (1972).

[47] C. Kalbach-Cline, Nucl. Phys. **A210**, 590 (1973).

[48] C.K. Cline, Nucl. Phys. **A186**, 273 (1972).

[49] L. Milazzo-Colli and G.M. Braga-Maracazzan, Nucl. Phys. **A210**, 297 (1973).

[50] F.C. Williams Jr., Nucl. Phys. **A166**, 231 (1971).

[51] Shi Xiangjun, H. Gruppelaar, And J.M. Akkermans, Nucl. Phys. **A466**, 333 (1987).

[52] J. Dobes and E. Betak, Z. Phys. **A310**, 329 (1983).

[53] C. Kalbach, Phys. Rev. **C33**, 818 (1986).

[54] M. Herman, G. Reffo, and C. Costa, Phys. Rev. **C39**, 1269 (1989).

[55] G. Mantzouranis, H.A. Weidenmüller, and D. Agassi, Z. Phys. **A276**,145 (1976).

[56] J.M. Akkermans, H. Gruppelaar, and G. Reffo, Phys. Rev. **C22**, 73 (1980).

[57] C. Kalbach, Phys. Rev. **C37**, 2350 (1988).

[58] M.C. Chadwick and P.Oblozinsky, Phys. Rev. **C46**, 2028 (1992).

[59] M.C. Chadwick and P.Oblozinsky, Phys. Rev. **C50**, 2490 (1994).

[60] K. Stankiewicz, A. Marcinkowski, and M. Herman, Nucl. Phys. **A536**, 67 (1992).

[61] P. Oblozinsky, Nucl. Phys. **A453**, 127 (1986).

[62] R. Bonetti, M.B. Chadwick, P.E. Hodgson, B.V. Carlson, and M.S. Hussein, Phys. Rep. **202**, 171 (1991).

[63] H. Feshbach, Ann. Phys. (NY) 159, 150 (1985).

[64] R. Bonetti, A.J. Koning, J.M. Akkermans and P.E. Hodgson, Phys. Rep. **247**, 1 (1994).

[65] A.J. Koning and M.B. Chadwick, Phys. Rev. **C56**, 970 (1997).

[66] N. Metropolis et al., Phys. Rev. **100**, 185 (1958); ibid, 204 (1958).

[67] H.W. Bertini, Phys. Rev. **131**,1801 (1963).

[68] M.L. Goldberger, Phys. Rev. **74**, 1269 (1948).

[69] A. Ferrari and P.R. Sala, in *Proceedings of the Workshop on Nuclear Reaction Data and Nuclear Reactors: Physics, Design and Safety* (1996), World Scientific, Singapore, (1998), p.424.

[70] M. Blann, Phys. Rev. Lett. **27**, 337 (1971).

[71] M. Blann, Phys. Rev. Lett. **28**, 757 (1972).

[72] M. Blann, Nucl. Phys. **A213**, 570 (1973).

[73] M. Blann, Phys. Rev. **C54**, 1341 (1996).

[74] M. Blann and M.B. Chadwick, Phys. Rev. **C57**, 233 (1998).

[75] M. Blann and H.K. Vonach, Phys. Rev. **C28**, 1475 (1983).